Guo et al. *Zool. Res.* 2024, 45(4): 924−936
https://doi.org/10.24272/j.issn.2095-8137.2024.034

ZR | Zoological Research

Article Open Access

Rotating magnetic field inhibits Aβ protein aggregation and alleviates cognitive impairment in Alzheimer's disease mice

Ruo-Wen Guo[1,2], Wen-Jing Xie[1,3], Biao Yu[1], Chao Song[1], Xin-Miao Ji[1], Xin-Yu Wang[1,3], Mei Zhang[4], Xin Zhang[1,2,3,*]

[1] *High Magnetic Field Laboratory*, *CAS Key Laboratory of High Magnetic Field and Ion Beam Physical Biology*, *Hefei Institutes of Physical Science*, *Chinese Academy of Sciences*, *Hefei*, *Anhui* 230031, *China*

[2] *Science Island Branch of Graduate School*, *University of Science and Technology of China*, *Hefei*, *Anhui* 230036, *China*

[3] *Institutes of Physical Science and Information Technology*, *Anhui University*, *Hefei*, *Anhui* 230601, *China*

[4] *School of Life Sciences*, *Division of Life Sciences and Medicine*, *University of Science and Technology of China*, *Hefei*, *Anhui* 230026, *China*

ABSTRACT

Amyloid beta (Aβ) monomers aggregate to form fibrils and amyloid plaques, which are critical mechanisms in the pathogenesis of Alzheimer's disease (AD). Given the important role of Aβ1-42 aggregation in plaque formation, leading to brain lesions and cognitive impairment, numerous studies have aimed to reduce Aβ aggregation and slow AD progression. The diphenylalanine (FF) sequence is critical for amyloid aggregation, and magnetic fields can affect peptide alignment due to the diamagnetic anisotropy of aromatic rings. In this study, we examined the effects of a moderate-intensity rotating magnetic field (RMF) on Aβ aggregation and AD pathogenesis. Results indicated that the RMF directly inhibited Aβ amyloid fibril formation and reduced Aβ-induced cytotoxicity in neural cells *in vitro*. Using the AD mouse model APP/PS1, RMF restored motor abilities to healthy control levels and significantly alleviated cognitive impairments, including exploration and spatial and non-spatial memory abilities. Tissue examinations demonstrated that RMF reduced amyloid plaque accumulation, attenuated microglial activation, and reduced oxidative stress in the APP/PS1 mouse brain. These findings suggest that RMF holds considerable potential as a non-invasive, high-penetration physical approach for AD treatment.

Keywords: Alzheimer's disease; Rotating magnetic field; Amyloid-β; Cognitive function; Alzheimer's disease animal models

INTRODUCTION

Alzheimer's disease (AD) is a chronic, incurable neurodegenerative condition and the most prevalent form of dementia worldwide, predominantly afflicting the elderly. Its primary clinical manifestations include cognitive and behavioral decline, memory recall impairments, and spatial perception difficulties, as well as changes in personality and disposition (Ballard et al., 2011; Graff-Radford et al., 2021). Advances in modern medicine have extended human lifespans, leading to a notable increase in age-related neurodegenerative disorders. At present, more than 55 million individuals worldwide are affected by AD and other types of dementia, with projections estimating a rise to 152 million by 2050 (Gauthier et al., 2021). This trend presents an increasingly critical public health challenge, imposing substantial socioeconomic and personal burdens on sufferers and their families (2023 Alzheimer's disease facts and figures, 2023).

The pathogenesis of AD is characterized by the presence of senile plaques and neurofibrillary tangles. These pathological changes are driven by the deposition of beta-amyloid protein and the entanglement of hyperphosphorylated tau (Blennow et al., 2006). Amyloid beta peptide (Aβ) is the primary cause of senile plaque formation, generated by the cleavage of amyloid precursor protein (APP) into peptide fragments predominantly composed of Aβ 1-40 and Aβ 1-42, which aggregate to form oligomers or fibrils (Bayer et al., 1999; Chen et al., 2017; Iwatsubo et al., 1995; Selkoe, 2001). Notably, Aβ oligomers exert neurotoxic effects that ultimately lead to neuronal cell death (Tiwari et al., 2019). Inhibition of Aβ accumulation within the central nervous system has been shown to effectively ameliorate cognitive deficits in mouse models of AD (Companys-Alemany et al., 2022; Fu et al., 2016; Zhang et al., 2019), demonstrating the therapeutic potential of reducing Aβ accumulation in AD treatment.

Magnetic fields possess the advantage of high penetration,

This is an open-access article distributed under the terms of the Creative Commons Attribution Non-Commercial License (http://creativecommons.org/licenses/by-nc/4.0/), which permits unrestricted non-commercial use, distribution, and reproduction in any medium, provided the original work is properly cited.

Copyright ©2024 Editorial Office of Zoological Research, Kunming Institute of Zoology, Chinese Academy of Sciences

Received: 05 April 2024; Accepted: 25 April 2024; Online: 26 April 2024

Foundation items: This study was supported by the National Key R&D Program of China (2023YFB3507004), National Natural Science Foundation of China (U21A20148), International Partnership Program of Chinese Academy of Sciences (116134KYSB20210052), Heye Health Technology Chong Ming Project (HYCMP2021010), and CASHIPS Director's Fund (BJPY2021A06)

*Corresponding author, E-mail: xinzhang@hmfl.ac.cn

allowing them to penetrate the whole body, including the brain. *In vitro* experiments have demonstrated that magnetic fields can affect the alignment of peptide dipoles, resulting in a reduction of the inherent beta-folding conformation (Todorova et al., 2016), considered an intermediate state in amyloid-like protein formation (Michaels et al., 2018; Todorova et al., 2016). The diphenylalanine (FF) sequence within KLVFF is critical for Aβ assembly and amyloid aggregation (Castelletto et al., 2017). The self-assembled tubular structures of FF align in high static magnetic fields due to the magnetic moments arising from the anisotropy of aromatic rings in peptide fragments (Hill et al., 2007). A moderate-intensity rotating magnetic field (RMF) generated by a pair of permanent magnets has been shown to agitate self-assembled β-peptide foldamers (Kwon et al., 2015). Thus, we hypothesize that applying a similar RMF may disrupt the Aβ assembly process, thereby reducing senile plaque formation.

In this study, we performed both *in vivo* and *in vitro* experiments to explore the potential application of RMF in AD. Our findings demonstrated that RMF significantly inhibited Aβ amyloid fibril formation and reduced cellular cytotoxicity *in vitro.* Moreover, *in vivo* animal behavior assessments and pathological examinations revealed the substantial potential of RMF in AD treatment.

MATERIALS AND METHODS

Preparation of Aβ peptide monomers

Aβ1-42 peptide (Sangon Biotech, China) was dissolved in 1,1,1,3,3,3-hexafluoro-2-propanol (HFIP) (1 mg/mL) and thoroughly dried under a nitrogen stream to obtain peptide films. The films were then dissolved in 10 mmol/L sodium hydroxide and further diluted with phosphate-buffered saline (PBS) to the desired experimental concentration. Control groups for all experiments were treated with PBS containing the same concentration of sodium hydroxide.

Cell culture

Neuroblastoma SH-SY5Y cells (ATCC) were cultured in a mixture of Minimum Essential Medium (MEM, Gibco, 2193264, USA) and Nutrient Mixture F12 (F12, Gibco, 2276977, USA) containing 10% fetal bovine serum (FBS) (CLARK Bioscience, FB 25015, USA). The cells were grown at 37°C under 5% CO_2 conditions and passaged every 3–4 days.

Animals

APP/PS1 mice are double transgenic mice expressing a chimeric mouse/human amyloid precursor protein (Mo/HuAPP695swe) and a mutant human presenilin 1 (PS1-dE9). All experimental mice were obtained from Nanjing GemPharmatech Co., Ltd. (China). The APP/PS1 mice were divided into sham and 0.4 T RMF groups, with age-matched C57 mice used as wild-type (WT) controls. Starting at 2 months of age, the APP/PS1 mice were exposed to 0.4 T RMF or sham treatment for 3–6 h/day, 5 days/week (Monday–Friday, 2–11 months old, 3 h/day; 11–14 months old, 6 h/day). The WT mice were raised in individual ventilated cages (IVC).

The study was conducted according to the National Institutes of Health Guide for the Care and Use of Laboratory Animals (NIH publication, 8th Edition, 2011). All procedures were approved by the Association of Laboratory Animal Sciences at Anhui Medical University (No. LLSC20232243).

RMF setup

The RMF equipment setup has been described previously (Ji et al., 2023). Briefly, the apparatus consisted of two assembled permanent magnets (N42M neodymium) fixed on a rotor, with the North and South poles oriented upwards. The magnets exhibited surface magnetic flux densities of approximately 1 T, and the rotor operated at a clockwise frequency of 4.2 Hz. For the sham group, two non-magnetized neodymium assemblies were used, rotating at the same frequency. The entire assembly was placed inside a square wooden box (44 cm×41 cm×52 cm).

For cellular and protein assays, both the magnetic field exposure and sham group samples were positioned on the surface of the wooden box, enclosed in customized 37°C incubators with a water bath, with or without a 5% CO_2 supply (Figure 1A). The maximum magnetic field intensity at the sample location was 0.4 T.

In animal experiments, cages for both the magnetic field exposure and the sham groups (two cages per group) were placed above the wooden boxes. The mice were then exposed to magnetic field or sham conditions for 3–6 h/day, 5 days/week over a period of 12 months. The maximum magnetic field intensity at the position of the mouse feet was 0.4 T.

Thioflavin T (ThT) assay

ThT powder (1.3 mg) was added to 15 mL of PBS solution to prepare a 275 μmol/L ThT stock solution. Aβ 1-42 monomer solution (10 μmol/L) was mixed with ThT solution (25 μmol/L) to a final volume of 200 μL in a 96-well plate. After 24 h of treatment at 37°C with either 0.4 T RMF or sham, fluorescence intensity was measured using a SpectraMax i3x plate reader (Molecular Devices, USA) with excitation and emission wavelengths of 440 nm and 480 nm, respectively (Liu et al., 2020).

Circular dichroism (CD) spectroscopy

Aβ1-42 solution (50 μmol/L) was treated with 0.4 T RMF or sham at 37°C for 24 h. The sample was then placed in a quartz cuvette and measured at room temperature using a J1 700 circular dichroism spectrometer (JASCO, Japan). Wavelengths were scanned from 190 nm to 260 nm at 1 nm intervals, with spectra averaged over three scans. CD curves were smoothed using GraphPad Prism v9.0 and analyzed using Spectra Manager v.2.0.

Dynamic light scattering (DLS)

Aβ1-42 solution (50 μmol/L) treated with 0.4 T RMF or sham (24 h, 37°C) was analyzed using a Zetasizer Nano-ZSE particle analyzer (Malvern Instrument, UK) with a laser source at λ=633 nm and a scattering angle of θ=173 degrees. Each sample was measured 10 times, and size distribution was plotted using GraphPad Prism v.9.0.

Dot blotting assay

Nitrocellulose membranes were cut into 1 cm pieces, onto which was spotted 2 μL of Aβ1-42 solution (50 μmol/L, treated with 0.4 T RMF or sham at 24 h and 37°C). The membranes were air-dried, and incubated with 5% bovine serum albumin for 30 min at room temperature, followed by incubation with A11 (Thermo Fisher, AHB0052, USA) (1:1 000) and 6E10 (Covance, SIG-39320, USA) antibodies (1:1 000) overnight at 4°C. The A11 antibody is specific to soluble oligomers (Pujadas et al., 2014) and the 6E10 antibody can detect all types of Aβ proteins (Yang et al., 2017). After washing with

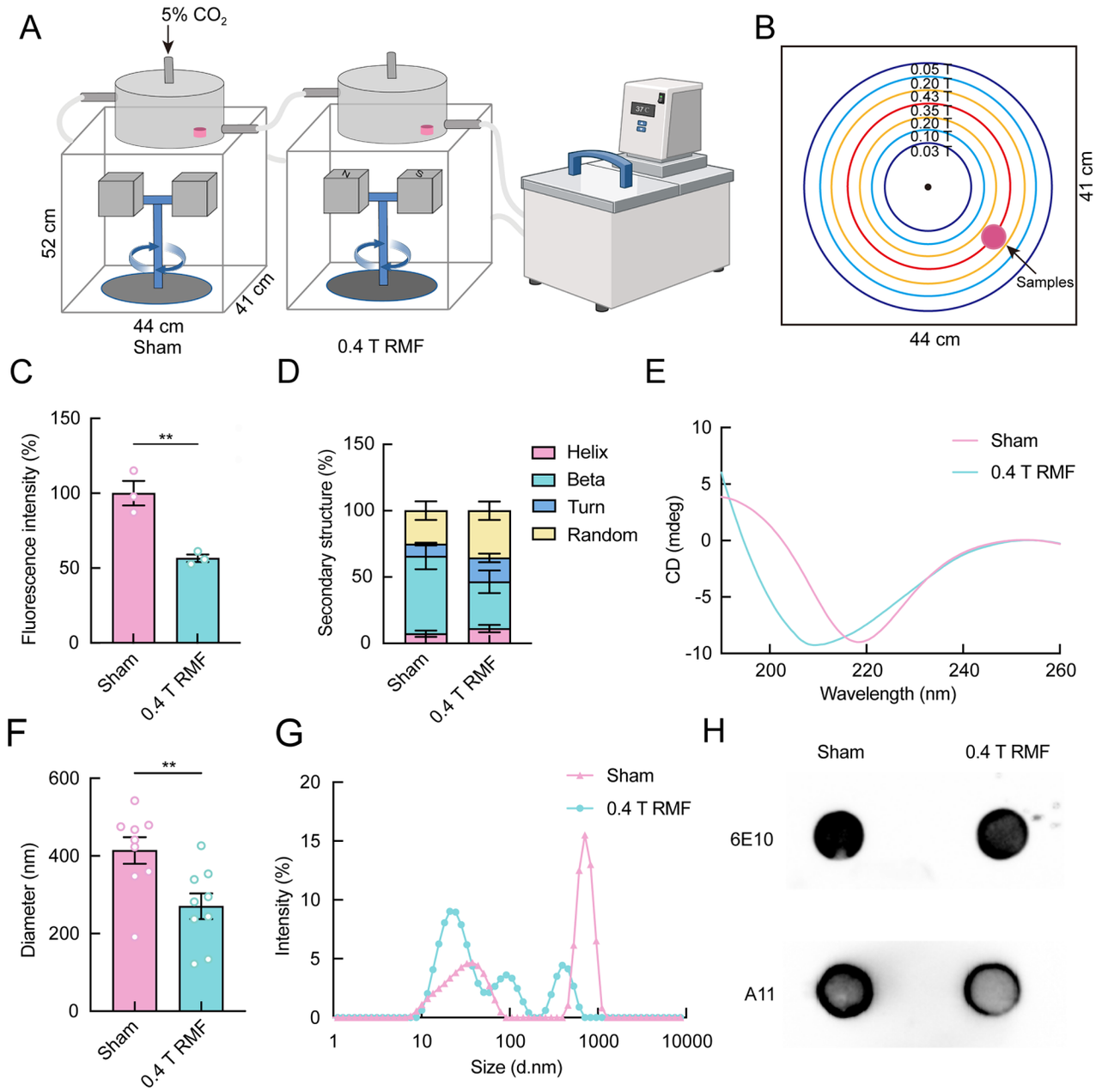

Figure 1 RMF inhibits Aβ amyloid fibril formation *in vitro*

A: Illustration of experimental setup for peptide and cellular experiments. Non-magnetized and magnetized neodymium were used to construct the sham and RMF instruments, respectively. Surface intensity of the magnetized neodymium for RMF was ~1 T, while the intensity at the experimental samples was ~0.4 T Max. B: Measured magnetic flux density distribution on the surface of the instrument. Cells and peptides were placed at the 0.4 T position for most experiments. C: Aβ1-42 aggregation was monitored by ThT fluorescence assay with and without 0.4 T RMF treatment. D: Distribution ratio of different protein structures in Aβ1-42 solution after 24 h of sham or 0.4 T RMF treatment. Data are mean±SEM, *n*=3. E: Circular dichroism spectra of Aβ1-42 solution treated with sham or 0.4 T RMF for 24 h. F: DLS measurement the Aβ1-42 particle size after 24 h of treatment with and without 0.4 T RMF. Data are mean±SEM, *n*=9. G: DLS showing particle size distribution of Aβ1-42 after sham or 0.4 T RMF treatment for 24 h. H: Representative dot blot bands of Aβ monomers and oligomers. *: P<0.05; **: P<0.01.

TBST, the membranes were incubated with secondary antibodies (1:1 000) for 40 min at room temperature. The membranes were then washed and exposed for chemiluminescent detection using an imaging system.

Cell viability assay

SH-SY5Y cells were seeded at a density of 1×10^4 cells/well in a 96-well plate overnight. After adhering, the medium was replaced with Aβ1-42 solution at different concentrations, and the cells were treated with 0.4 T RMF and sham for 24 h. Cell viability was detected using a Cell Counting Kit-8 (CCK-8) (MedChemExpress, HY-K0301, USA). After incubating each well with 10 μL of CCK-8 solution for 1 h, absorbance was measured at 450 nm using a SpectraMax i3x plate reader (Molecular Devices, USA).

Cell live/dead staining

Cells were seeded in small culture plates (0.8 cm diameter) and treated with or without Aβ1-42. After RMF treatment for different durations, the cells were collected and centrifuged at

1 000 ×*g* for 5 min at room temperature. An appropriate volume of calcein acetoxymethyl ester (calcein AM)/propidium iodide (PI) detection working solution was then added according to the manufacturer's instructions. The samples were then incubated at 37°C in the dark for 30 min before analysis using a fluorescence microscope (Olympus, SZX10, Japan).

Flow cytometry apoptosis analysis

SH-SY5Y cells were seeded at a density of 3×10^5 cells/dish in a cell culture dish (3 cm diameter) and incubated overnight at 37°C. After adhering, the medium was replaced with Aβ1-42 solution (20 μmol/L) and the cells were treated with 0.4 T RMF or sham for 24 h. Apoptosis was detected using an Annexin V-FITC Apoptosis Detection Kit (BD Biosciences, 0076884, USA). Flow cytometry was performed using a Cyto FLEX flow cytometer (Beckman Coulter, USA).

Open field test (OFT)

Mice were placed in a white polyvinyl chloride (PVC) open field apparatus (SA215, SANS, China), consisting of a square area divided into four equal zones (40 cm×40 cm×40 cm (length×width×height)), with a central area (30 cm×30 cm (length×width)) and a peripheral area. The apparatus was cleaned before each trial, and the mice were placed in the center of the square. The ANY-Maze Video Tracking System (Stoelting, USA) was used to record the movement trajectories of mice within the central area for 5 min, measuring movement distance, average movement speed, and time spent in the central area.

Novel object recognition test (NORT)

After a 24 h interval following the OFT, the mice were returned to the same square area. Two identical objects in shape and color were placed within the area, and the mice were allowed to explore these objects for 10 min. After 2 h, one of the objects was replaced with a new object (different shape and color), and the mice were again allowed 10 min to explore. During training, the time spent exploring the familiar object was denoted as T1, and the time spent exploring the novel object was denoted as T2. The recognition index (RI) was calculated using the formula to assess the cognitive level of the mice:

$$RI = T2/(T1+T2)\times 100\% \quad (1)$$

Morris water maze (MWM) experiment

The experiment was conducted in a circular water pool (SA201, SANS, China) filled with non-toxic water containing white dye, maintained at 25°C, with a diameter of 120 cm. A movable circular platform (8 cm diameter) was submerged 1.5 cm beneath the surface of the water within the target quadrant. During the initial training phase, mice were placed randomly into the pool from four different directions and given 60 s to locate the hidden platform. If a mouse failed to find the platform within the allotted time, it was guided to the platform and allowed to remain there for around 15 s. This training was conducted over 5 days, with time taken to find the platform, swimming speed, and swimming path recorded. On day 6, the platform was removed, and the mice were placed in the pool from the opposite direction to the original platform location and given 60 s to find the original platform position. Movement, time taken to reach the target quadrant, and former location of the platform were recorded within 60 s. The ANY-Maze Video Tracking System (Stoelting, USA) was used to record data during the test period. Movement paths were analyzed using Pathfinder (Cooke et al., 2019).

Immunofluorescence: Following anesthesia, mice were perfused with saline, followed by 4% paraformaldehyde (PFA). Organ tissues were placed in 4% PFA at 4°C overnight. A semi-automatic microtome (Leica Biosystems RM2245, Germany) was used to section the tissues into 5 μm slices for subsequent experiments. Mouse brain tissue sections were permeabilized with 0.5% Triton X-100 for 10 min at room temperature. After blocking, the sections were incubated overnight at 4°C with antibodies 6E10 (1:500) and IBA1 (1:500). The following day, the sections were incubated with secondary antibodies (1:1 000) for 1 h at room temperature, and 4',6-diamidino-2-phenylindole (DAPI) was used to stain the cell nuclei. Finally, the sections were examined under a Nikon TS100 microscope (Nikon, Japan).

Thioflavin S (Thio S) staining: After dewaxing, brain tissue sections were washed, incubated with 0.5% Thio S dissolved in 50% ethanol for 20 min at room temperature, washed twice in 80% ethanol (10 s each time), and finally rinsed with ddH_2O. After mounting, the sections were examined under a Nikon TS100 microscope (Nikon, Japan).

Hematoxylin and eosin (H&E) staining: After dewaxing, mouse organ sections were stained with H&E, decolorized with alcohol, rinsed with water, and subjected to ethanol dehydration. Finally, the sections were mounted and examined under a Nikon TS100 microscope (Nikon, Japan).

Nonalcoholic fatty liver disease (NAFLD) activity score (NAS): The NAS was used to assess NAFLD severity, providing a semiquantitative assessment of four histological features: steatosis (0–3), lobular inflammation (0–2), hepatocyte ballooning (0–2), and fibrosis (0–4) (Kleiner et al., 2005).

Oil red O staining: Mouse liver tissues were embedded in optical coherence tomography (OCT) compound, and frozen slices (5 μm) were prepared at −20°C. A saturated Oil Red O solution was dissolved in isopropyl alcohol and distilled water at a ratio of 3:2 (v:v). After filtration, frozen sections were stained in dilute Oil Red O solution for 6 h at room temperature. The sections were then rinsed with 60% isopropyl alcohol aqueous solution three times and running water once. The frozen sections were counterstained with hematoxylin solution for 1–2 min and washed with water. The stained sections were sealed with neutral gelatin and photographed using a Nikon TS100 microscope (Nikon, Japan).

Enzyme linked immunosorbent assay (ELISA): Malondialdehyde (MDA) and superoxide dismutase (SOD) levels in the mouse hippocampus and medial prefrontal cortex (mPFC) were determined according to the manufacturer's instructions (Aimeng Youning, China). Absorbance was measured at 450 nm using a SpectraMax i3x plate reader (Molecular Devices, USA).

RNA sequencing (RNA-seq) analysis: After anesthesia, the mice were perfused with saline, and hippocampal tissue was isolated and stored at −80°C. Total RNA was extracted using Trizol (15596018, Thermo Fisher, USA). Transcriptomic analysis was conducted by LC-BioTechnology (China). The generated transcriptome data were processed using StringTie and Ballgown to calculate fragments per kilobase million (FPKM) values for assessing gene expression levels. Gene Ontology (GO) enrichment analysis of differentially expressed genes (DEGs) was also conducted by LC-BioTechnology Co.,

Ltd. (https://www.omicstudio.cn/tool).

Statistical analysis

All statistical analyses were performed using GraphPad Prism v.9.0. Experimental data are presented as mean±standard error of the mean (SEM). One-way or two-tailed unpaired *t*-tests were used to calculate *P*-values for comparisons. $P<0.05$ was considered statistically significant.

RESULTS

0.4T RMF inhibits Aβ amyloid fibril formation *in vitro*

To elucidate the impact of RMF on Aβ amyloid aggregation, we used RMF instruments consisting of a pair of neodymium magnets, with non-magnetized neodymium serving as a sham control, and equipped with a temperature and gas control system (Figure 1A) (Ji et al., 2023). The Aβ1-42 solution was placed in the instrument, with a magnetic field intensity of approximately 0.4 T in the RMF group (Figure 1B). The presence of β-folded structures, characteristic of amyloid proteins, was assessed using ThT fluorescence analysis, a widely adopted method for amyloid fibril identification (Abeyawardhane et al., 2018; Younan & Viles, 2015). Results showed that the ThT fluorescence intensity of the Aβ1-42 solution treated with 0.4 T RMF decreased by about 43% compared to the sham group (Figure 1C). Given that the progression of Aβ aggregation from soluble monomers to insoluble fibrils involves a conformational shift from α-helices to β-sheets (Ding et al., 2003), CD spectra were employed to examine the distribution of protein secondary structures in Aβ1-42 monomer solutions (100 μmol/L). The sham group primarily exhibited β-sheets as the secondary structure, accounting for approximately 58.3%. In contrast, the β-sheets content of the Aβ1-42 monomer solution treated with 0.4 T RMF decreased by 25.2% compared to the sham group (Figure 1D, E). The DLS experiments revealed that the average particle diameter of the Aβ1-42 solution (100 μmol/L) treated with 0.4 T RMF was smaller than that of the sham group (Figure 1F). Additionally, the sham group exhibited a higher percentage of protein distribution in the large diameter area (Figure 1G). Dot blotting revealed a higher A11 level in the sham group compared to the 0.4 T RMF group (Figure 1H). These findings demonstrate the ability of 0.4 T RMF to inhibit the aggregation of Aβ1-42 monomeric protein under *in vitro* conditions at 37°C.

0.4T RMF mitigates Aβ-induced cytotoxicity *in vitro*

We conducted *in vitro* experiments using the human neuroblastoma cell line SH-SY5Y to evaluate the effects of RMF on Aβ1-42-induced cytotoxicity, as depicted in Figure 1A. Before RMF exposure, the SH-SY5Y cells were treated with different concentrations of Aβ1-42 protein monomer solution, and relative cell viability was determined after 24 h of incubation at 37°C. Results show that the relative cell viability decreased with increasing concentrations of Aβ1-42 monomer solution: 85.85% (5 μmol/L), 81.17% (10 μmol/L), 77.90% (20 μmol/L), and 68.17% (40 μmol/L) (Figure 2A). A

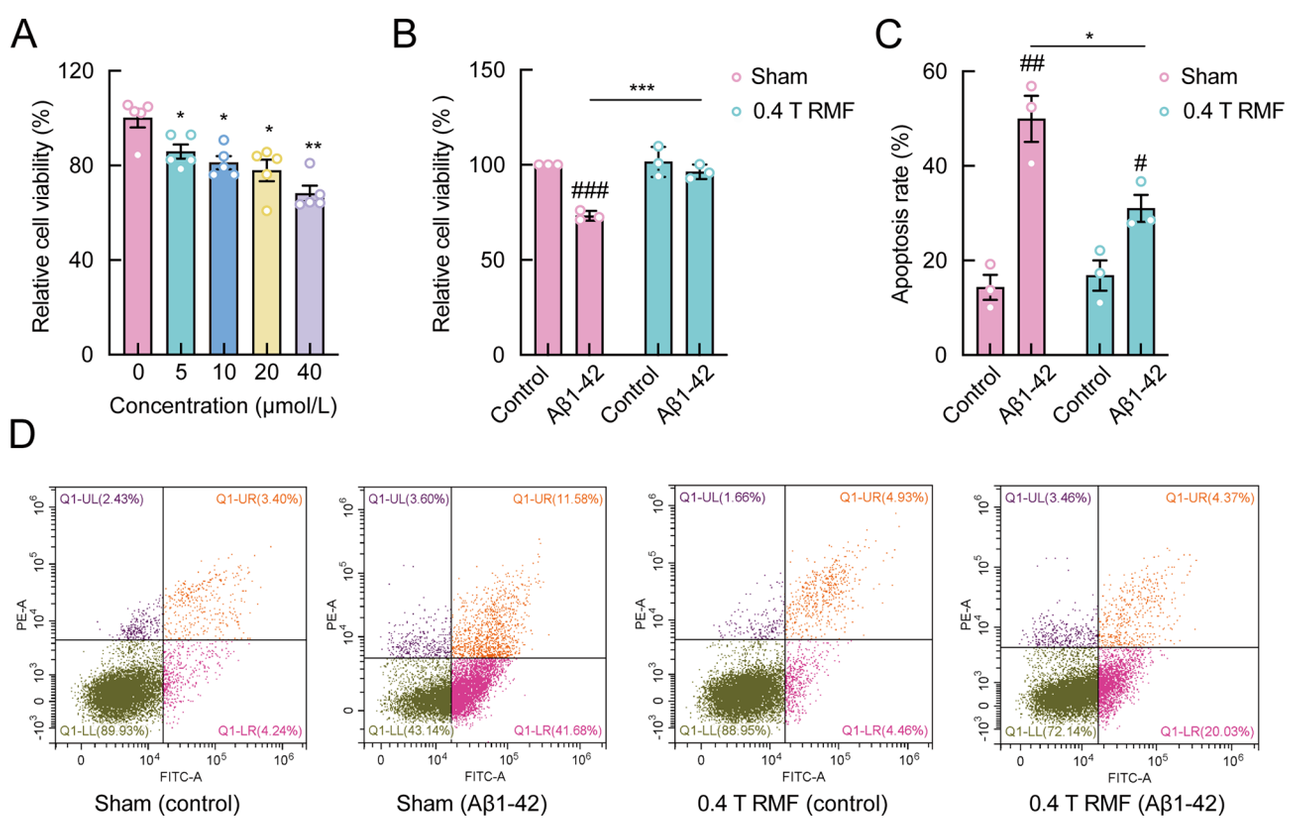

Figure 2 RMF reduces Aβ-induced cytotoxicity *in vitro*

A: Cell viability of SH-SY5Y cells treated with different concentrations of Aβ1-42 solution after 24 h. Data are mean±SEM, $n=5$. *: $P<0.05$; **: $P<0.01$. B: Viability of SH-SY5Y cells treated with or without Aβ1-42 solution (20 μm) after treatment with sham or 0.4 T RMF for 24 h. C: Apoptosis rate of SH-SY5Y cells treated with or without Aβ1-42 solution (20 μm) after treatment with sham or 0.4 T RMF for 24 h. Data are mean±SEM, $n=3$. *: $P<0.05$; **: $P<0.01$; $^{\#}$: $P<0.05$, and $^{\#\#}$: $P<0.01$ compared to control group. D: Representative flow cytometry images of sham and 0.4 T RMF-treated Aβ1-42 solution after 24 h.

concentration of 20 μmol/L was selected for subsequent experiments. Live/dead staining with calcein-AM and PI was performed to differentiate between live and dead cells. SH-SY5Y cells treated with Aβ1-42 and exposed to 0.1 T or 0.4 T RMF exhibited higher cell viability compared to the sham group, consistently observed across all three timepoints tested (24, 48, and 72 h). Notably, the 0.4 T RMF group showed greater cell viability than the 0.1 T RMF group (Supplementary Figure S1). Specifically, treatment with 0.4 T RMF increased SH-SY5Y cell viability by 23.1% compared to the sham group (Figure 2B). Additionally, flow cytometry revealed a 19.6% reduction in apoptosis in cells treated with 20 μmol/L Aβ monomer solution and exposed to 0.4 T RMF (Figure 2C, D). These results indicate that 0.4 T RMF can reduce Aβ1-42 aggregate-induced cytotoxicity in SH-SY5Y cells.

0.4T RMF improves motor and exploration abilities in APP/PS1 mice

We further examined the impact of RMF on reducing Aβ1-42 aggregation in the brains of 2-month-old male APP/PS1 mice based on *in vivo* experiments (Figure 3A). The mouse cages were positioned on the RMF and sham instruments, as described previously (Ji et al., 2023). After 12 months of RMF exposure, no significant differences in body weight were observed (Supplementary Figure S2A). The APP/PS1 mice consumed slightly more food and water compared to the WT group (Supplementary Figures S2B, C). In the OFT and NORT (Figure 3B) experiments, no significant differences were detected in motor, exploratory, or non-spatial memory abilities among the three groups at 2 months of age. However, the APP/PS1 mice appeared more active than the WT healthy mice (Supplementary Figure S3A–D), possibly due to aggressive behavior (Pugh et al., 2007). At 6 months of age, no obvious differences in behavioral tests were observed among the three groups (Supplementary Figure S3E–H). At 11 months of age, there was a non-significant trend towards improved motor, exploratory, and non-spatial memory abilities in the RMF group compared to the sham group (Supplementary Figure S3I–L). Therefore, we increased the RMF exposure time from 3 h/day to 6 h/day (5 days/week). At 14 months, the RMF-treated mice exhibited restored motor, exploration, and non-spatial memory abilities, similar to the WT healthy group (Figure 3C, D). In the OFT, the RMF group showed significantly higher time in the center area, total distance traveled, and mean speed compared to the sham group (Figure 3E–G). Based on the NORT, the cognitive index of the RMF group reached levels similar to the WT healthy group, with significantly improved recognition memory compared to the sham group (Figure 3H).

0.4T RMF significantly alleviates spatial memory impairments in APP/PS1 mice

We employed the MWM to assess the spatial learning and memory abilities of the APP/PS1 mice (Figure 4A). Following RMF exposure, the 14-month-old APP/PS1 mice exhibited improved escape latency compared to the sham group (Figure 4B). During the learning phase (days 1–5), no significant differences were observed in swimming speed or distance among the three groups (Figure 4C, D). However, the RMF group exhibited significantly restored memory and spatial learning abilities on day 6 (Figure 4E–H). The MWM trajectories are shown in Figure 4J. We performed subsequent analysis of the search strategies of mice after the learning phase (days 1–5). Using Pathfinder, we categorized all mouse movements into nine search strategies (Figure 4I) (Brody & Holtzman, 2006). Analysis revealed a daily increase in effective strategies in the WT and RMF groups over the five training days, whereas the sham group demonstrated a decline in effective training strategies on days 4 and 5 (Figure 4K). These findings indicate that after 12 months of RMF treatment, spatial memory and learning abilities were restored in APP/PS1 mice, suggesting the potential of RMF in alleviating cognitive impairments in AD mice.

0.4T RMF reduces amyloid plaque deposition and microglial activation in the brains of APP/PS1 mice

We performed Thio S staining to examine amyloid plaques in the brains of APP/PS1 mice. Results revealed reduced deposition of Aβ1-42 protein in both the mPFC (Figure 5A, B) and hippocampus (Figure 5C, D) of APP/PS1 mice treated with RMF. Given that abnormal morphology and proliferation of microglia are characteristic of AD histopathology (Hansen et al., 2018; Hickman et al., 2008), we used specific antibodies for Iba-1 to label microglia and 6E10 to label amyloid plaques. In the sham group, the mPFC and hippocampus of APP/PS1 mice exhibited extensive microglial activation and Aβ protein accumulation. In contrast, RMF treatment significantly reduced 1ba1 activation and Aβ protein aggregation in these brain regions (Figure 5E–H, Supplementary Figures S4A–D). In summary, treatment of APP/PS1 mice with RMF for 12 months reduced the deposition of Aβ protein and decreased microglial activation in the brains of APP/PS1 mice.

0.4T RMF reduces oxidative stress in APP/PS1 mouse brains and lipid deposition in the liver

To explore the mechanisms underlying the reduction of Aβ aggregation in the brains of AD mice, we isolated hippocampal tissue from APP/PS1 mice and conducted RNA-seq analysis. Results identified 564 up-regulated and 700 down-regulated DEGs in the hippocampal tissue after RMF treatment compared to the sham group (Figure 6A). GO enrichment analysis indicated that RMF treatment was associated with signaling pathways related to apoptosis, consistent with our previous experimental results. Moreover, GO pathway analysis suggested that RMF affected signaling pathways related to oxidative stress and lipid metabolism (Figure 6B). The gene heatmap indicated significant differences in genes related to these pathways (Figure 6C–E). Furthermore, several differences in the expression of genes associated with AD were detected (Figure 6F).

To investigate the association between oxidative stress and RMF, we quantified oxidative stress levels in the hippocampus of mice using ELISA. Results showed that MDA levels were higher in the hippocampus of the sham group compared to the WT group, while the RMF-treated APP/PS1 mice showed reduced MDA levels (Figure 6G). Conversely, SOD levels were lower in the sham group compared to the WT group, while the RMF-treated group displayed an ascending trend (Figure 6H).

Additionally, lipid accumulation and ballooning degeneration were prominent in the livers of APP/PS1 mice in the sham group. Interestingly, RMF-treated mice exhibited significantly reduced lipid accumulation, nearly reaching levels observed in healthy mice. Evaluation of NAS revealed significantly higher scores in the sham group, while RMF-treated mice exhibited scores similar to the WT group (Figure 6I, K). Additionally, oil red O staining confirmed the substantial reduction of lipid accumulation in the livers of RMF-treated APP/PS1 mice

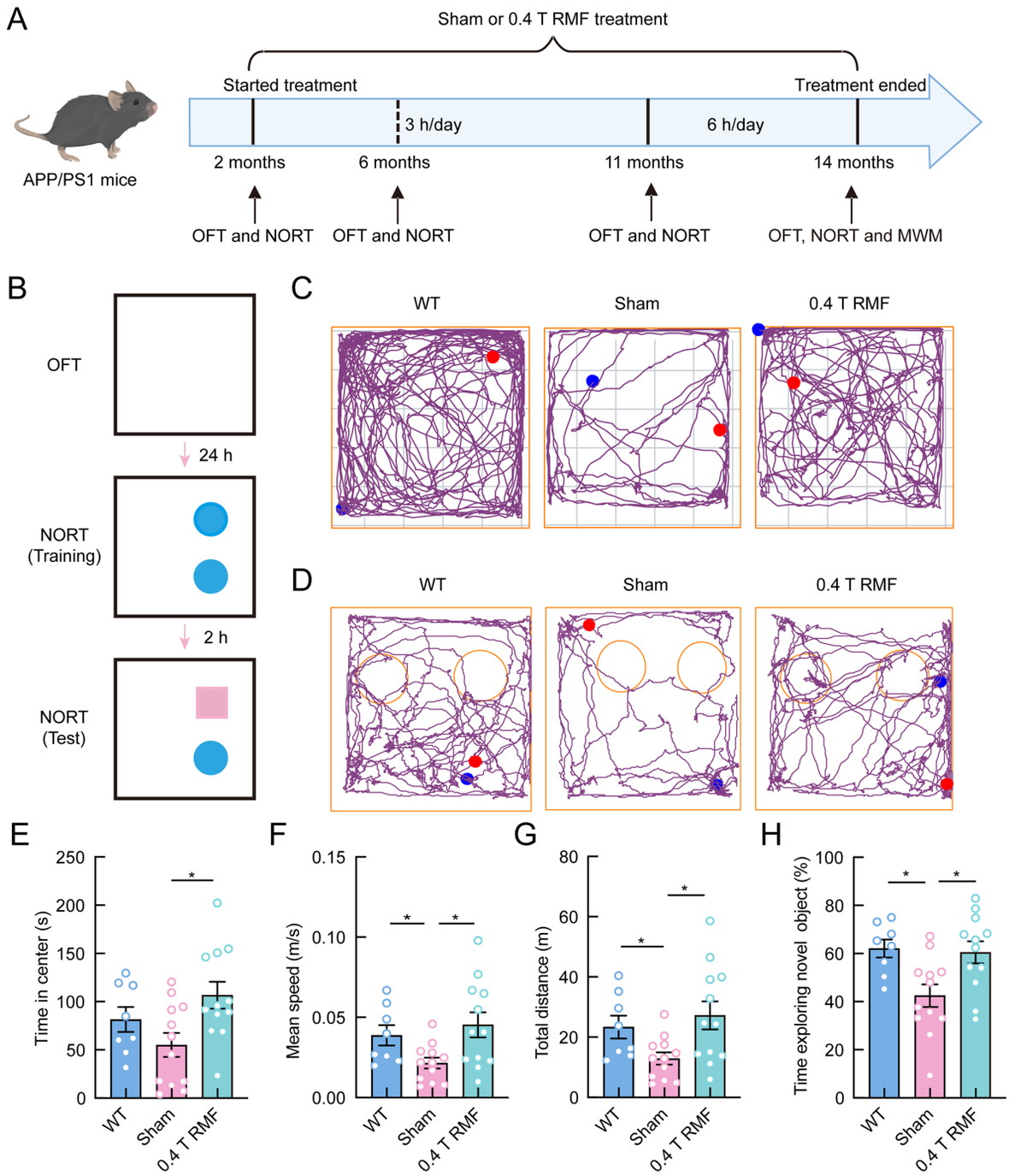

Figure 3 RMF improves motor and exploration abilities in APP/PS1 mice

A: Experimental design. APP/PS1 mice were exposed to a sham or RMF device for 12 months, with magnetic field exposure of 3 h/day (weekdays) from 2–11-months-old and 6 h/day (weekdays) from 11–14-months-old. Behavioral experiments were conducted at 2-, 11-, and 14-months-old. B: Illustration of OFT and NORT device. C: Representative mouse trajectories in OFT. D: Representative mouse trajectories in NORT. E–H: Behavioral tests at 14-months-old. E: Time spent by mice exploring central area in OFT. F: Average movement speed of mice in OFT. G: Total movement distance of mice in OFT. H: Percentage of time spent exploring novel objects in NORT. Data are mean±SEM, WT group, n=8; Sham and RMF group, n=12). *: P<0.05; **: P<0.01.

(Figure 6J, L). No significant differences were observed in the heart, spleen, or lung tissues among the three groups of mice (Supplementary Figure S5). This suggests that treatment with RMF may alleviate damage in the liver, brain and kidney tissues of APP/PS1 mice.

DISCUSSION

AD is one of the most prevalent neurodegenerative ailments linked with aging (Singh, 2020) and has been a focal point for diverse therapeutic strategies in clinical contexts spanning several decades (Andrieu et al., 2015; Fish et al., 2019). Most drugs approved by the US Food and Drug Administration (FDA) for treating AD aim to alleviate symptoms without altering disease progression and are accompanied by side effects such as headaches and nausea (2023 Alzheimer's disease facts and figures, 2023). Additionally, their effectiveness is limited by issues such as poor solubility and

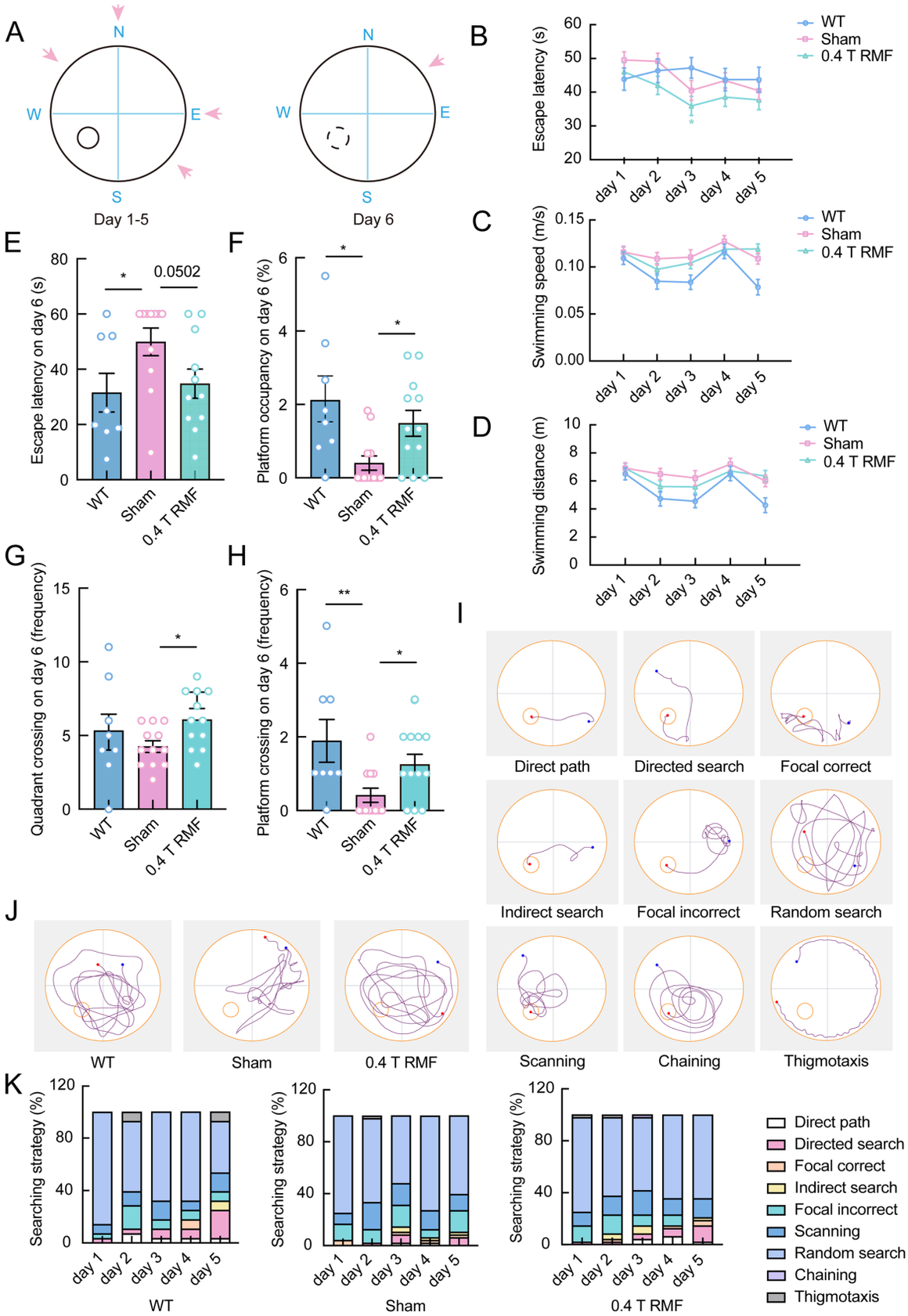

Figure 4 RMF significantly alleviates spatial memory impairments in APP/PS1 mice

A: Illustration of MWM device. B: Escape latency during training days. C: Swimming speed during training days. D: Swimming distance during training days. E: Escape latency during probe trial. F: Percentage of time spent on platform during probe trial. G: Number of platform crossings during probe trial. H: Number of target quadrant crossings during probe trial. I: Different types of search strategies during training days. J: Representative mouse trajectories in MWM. K: Percentage of different search strategies. Data are mean±SEM, WT group, n=8; Sham and RMF group, n=12). *: P<0.05, **: P<0.01.

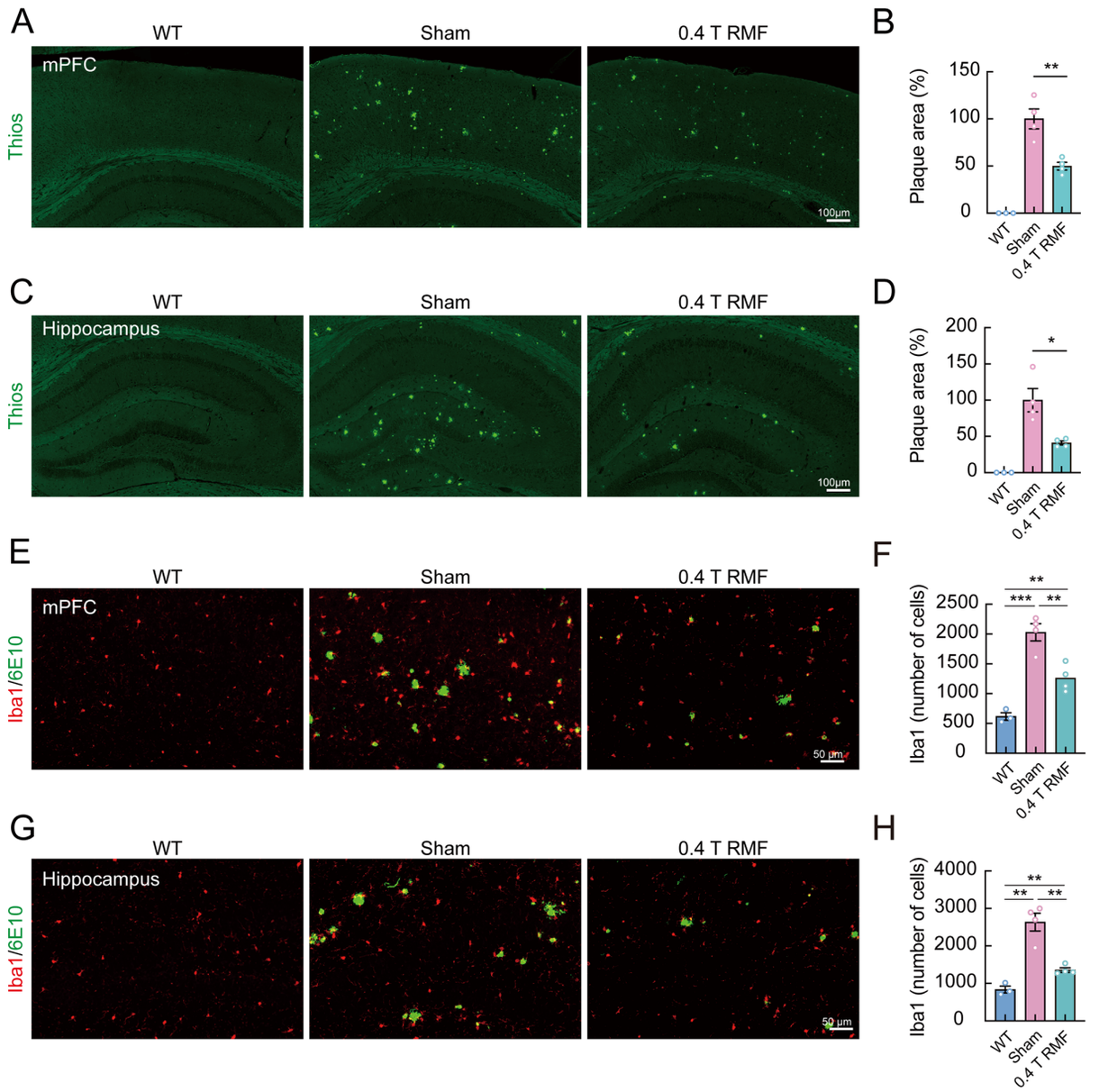

Figure 5 RMF reduces amyloid plaque deposition and microglial activation in APP/PS1 mouse brain

A: Thio S staining in mPFC of WT, sham, and 0.4 T RMF-treated groups. B: Relative area of Aβ plaque in mPFC of WT, sham, and 0.4 T RMF-treated groups. C: Thio S staining in hippocampus of WT, sham, and 0.4 T RMF-treated groups. D: Relative area of Aβ plaque in hippocampus of WT, sham, and 0.4 T RMF-treated groups. E: Immunofluorescence with anti-Iba1 (red) and E610 (green) antibody in mPFC of WT, sham, and 0.4 T RMF-treated groups. F: Number of Iba1-positive microglia in mPFC of WT, sham, and 0.4 T RMF-treated groups. G: Immunofluorescence with anti-Iba1 (red) and E610 (green) antibodies in hippocampus of WT, sham, and 0.4 T RMF-treated groups. H: Number of Iba1-positive microglia in hippocampus of WT, sham, and 0.4 T RMF-treated groups. Data are mean±SEM, WT group, n=3; Sham and RMF group, n=4). *: P<0.05; **: P<0.01.

difficulty in crossing the blood-brain barrier (BBB) (Karthivashan et al., 2018). Nonpharmacological interventions are commonly used to alleviate agitation and aggressive behavior in AD patients, often proving more effective and safer than pharmacological interventions (2023 Alzheimer's disease facts and figures, 2023). Research has shown that magnetic fields, such as electromagnetic fields and transcranial magnetic stimulation, may reduce neuronal damage and cognitive impairment in AD (Arendash et al., 2010; Huang et al., 2017). Although prolonged exposure to high-gradient magnetic fields has been shown to have adverse effects on severely diabetic mice (Yu et al., 2023), moderate-intensity RMF is not associated with any reported side effects. Based on *in vivo* and *in vitro* experiments, we discovered that RMF can disrupt Aβ assembly and reduce amyloid plaque deposition in the brains of AD mice, which restored motor ability and significantly alleviated cognitive impairment (Figure 7).

We propose two primary mechanisms by which RMF affects Aβ assembly. The first mechanism involves diamagnetic anisotropy of the peptide. Aβ (1-42) monomers, comprising 42 amino acid residues, feature two α-helix segments linked by a regular type I β-turn structure (Kaur et al., 2020). Peptide bonds exhibit inherent diamagnetic anisotropy, generating torque that align proteins within a magnetic field. When peptide bonds are organized within a uniform structural

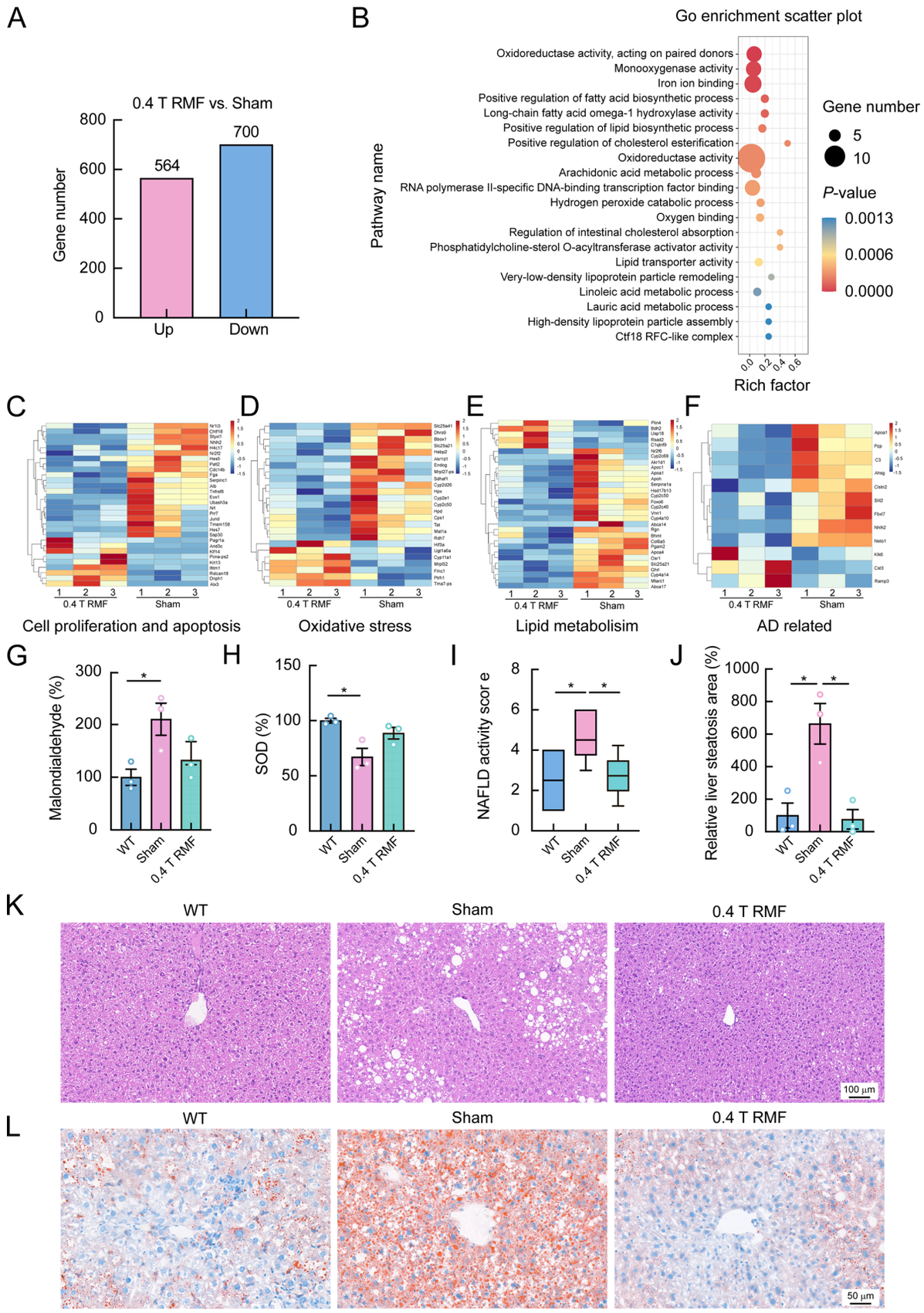

Figure 6 RMF reduces oxidative stress in APP/PS1 mouse brain and lipid deposition in the liver

A–F: Gene number, GO term, and heatmap of differentially expressed genes (DEGs) in the hippocampus of 14-month-old APP/PS1 mice after treatment with sham or RMF, revealed by RNA-seq. G, H: ELISA measurement of MDA and SOD levels. I, J: NAS and relative steatosis area in the liver of WT, sham, and RMF-treated mice. K: Representative images of H&E staining of liver of WT, sham, and RMF-treated mice. L: Representative images of oil red O staining of liver of WT, sham, and RMF-treated mice. Data are mean±SEM, n=3. *: P<0.05; **: P<0.01.

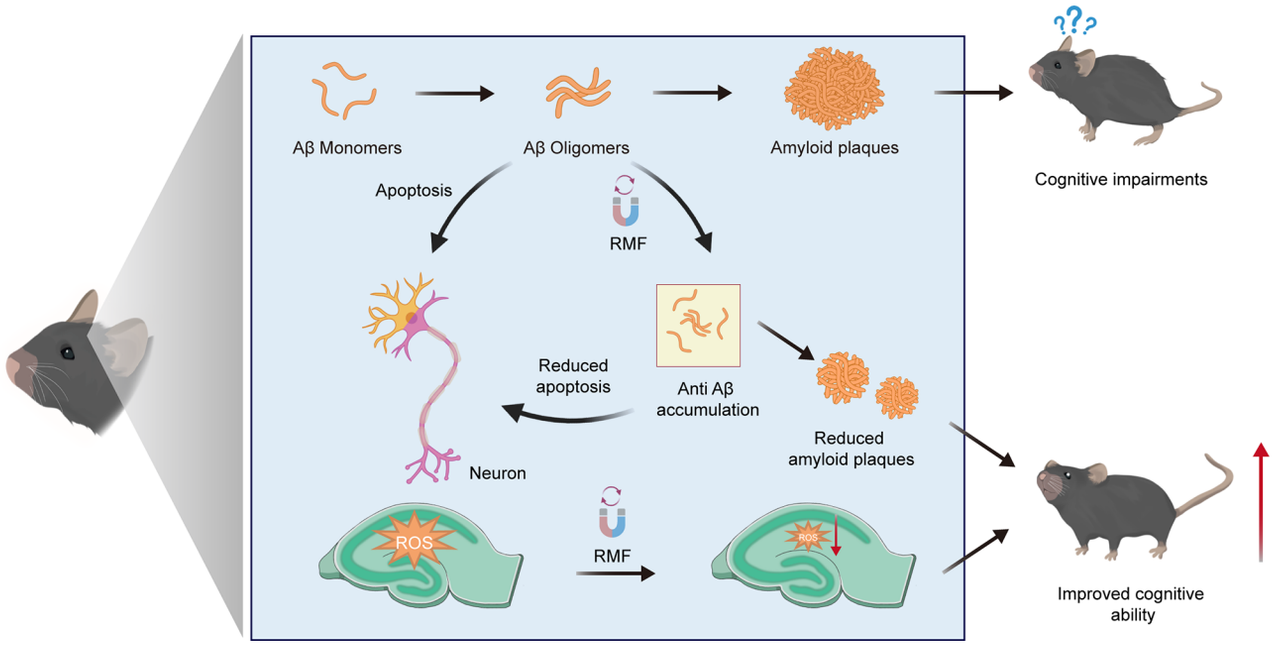

Figure 7 RMF reduces Aβ protein aggregation and alleviates cognitive impairment in AD mice

feature (α-helix or β-sheet), the cumulative anisotropy reflects the diamagnetic magnetization of each peptide bond (Pauling, 1979). These factors may induce shifts in the arrangement and orientation of Aβ protein monomers under RMF, ultimately impeding their aggregation.

The second mechanism involves the induced electric field. Saikia et al. (2019) proposed that low-intensity electric fields can suppress peptide aggregation without affecting their natural structure, whereas static magnetic fields of approximately 0.8 T show minimal ability to induce conformational changes. Furthermore, they stated that electromagnetic fields can align large molecules or dipoles along the axis of the applied field (Saikia et al., 2019). Our preliminary studies using the same set of devices demonstrated that RMF can hinder F-actin assembly via induced electric fields, effectively inhibiting breast cancer cell adhesion, migration, and metastasis in mice (Ji et al., 2023). This observation sparked our curiosity in determining whether RMF can also impede Aβ aggregation, a self-assembling protein. We hypothesize that RMF-induced electric fields can directly interact with molecular dipole moments to disrupt Aβ aggregation.

Furthermore, we propose that the alleviating effects of RMF on AD mice may be caused by multiple reasons, not limited to Aβ assembly. Firstly, our results indicated that RMF treatment reduced oxidative stress levels in the hippocampus of APP/PS1 mice. Aggregation of Aβ protein can cause oxidative stress and promote cell apoptosis. Oxidative stress accelerates AD progression by damaging intracellular macromolecules and regulating the post-translational modification of APP protein and the activity of its secreted enzymes (Lehtinen & Bonni, 2006; Schieber & Chandel, 2014). Several studies have shown that magnetic fields can lower oxidative stress levels in cells and mouse tissues (Feng et al., 2022; Frachini et al., 2024). Thus, the reduction of oxidative stress likely contributes significantly to the positive effects of RMF on AD mice. Secondly, our results also showed that RMF affected lipid metabolism, leading to notable changes in the liver. However, the primary effect of RMF on AD mice seems to be the inhibition of Aβ protein aggregation, as shown by both *in vivo* and *in vitro* experiments, rather than changes in lipid metabolism. Despite this, we cannot exclude the potential contribution of lipid metabolism in AD. Future studies using more specialized devices are necessary to dissect the relative contributions of the brain versus the liver.

Our study has some limitations. Firstly, due to the constraints with the RMF instruments, we were unable to test other RMF parameters. Future research should explore whether different field strengths and frequencies, combined with shorter treatment durations, could enhance therapeutic effects. We hope this will encourage further investigation into the use of magnetic fields for treating neurodegenerative diseases, exploring a variety of intensities and frequencies for potential clinical applications. Secondly, space limitations in the animal facility restricted our study to a single AD model (APP/PS1 mice). Future studies should include more mouse models, such as five familial AD (5×FAD) mice, which express human APP and PSEN1 transgenes with a total of five AD-linked mutations. Thirdly, our study only included male mice. Given the higher incidence of AD in females, it is crucial to examine sex-specific differences in responses to RMF treatment.

In conclusion, our findings suggest that intermittent exposure to moderate-intensity RMF holds promise as a non-invasive, high-penetration physical therapy for AD, capable of alleviating neuronal damage and cognitive impairment. While multiple factors contribute to the development of AD, we are optimistic that this “incurable” disease may eventually become preventable or manageable. RMF, either alone or in combination with other pharmaceutical or dietary interventions, could represent a novel treatment strategy worth exploring in future studies.

DATA AVAILABILITY

The data presented in the study have been deposited in the National Genomics Data Center (NGDC) (accession number: CRA016912), Science Data Bank (https://doi.org/10.57760/sciencedb.07903), and NCBI database (accession number: GSE269222).

SUPPLEMENTARY DATA

Supplementary data to this article can be found online.

COMPETING INTERESTS

The authors declare that they have no competing interests.

AUTHORS' CONTRIBUTIONS

X.Z. and R.W.G. designed the experiments. R.W.G., W.J.X., B.Y., S.C., X.M.J., X.Y.W., and M.Z. performed the experiments. X.Z. and R.W.G. wrote the manuscript with editing by all authors. All authors read and approved the final version of the manuscript.

ACKNOWLEDGMENTS

We thank Ding Joe Wang for cartoon illustrations.

REFERENCES

[Anonymous]. 2023. 2023 Alzheimer's disease facts and figures. *Alzheimer's & Dementia*, **19**(4): 1598–1695.

Abeyawardhane DL, Fernández RD, Murgas CJ, et al. 2018. Iron redox chemistry promotes antiparallel oligomerization of α-synuclein. *Journal of the American Chemical Society*, **140**(15): 5028–5032.

Andrieu S, Coley N, Lovestone S, et al. 2015. Prevention of sporadic Alzheimer's disease: lessons learned from clinical trials and future directions. *The Lancet Neurology*, **14**(9): 926–944.

Arendash GW, Sanchez-Ramos J, Mori T, et al. 2010. Electromagnetic field treatment protects against and reverses cognitive impairment in Alzheimer's disease mice. *Journal of Alzheimer's Disease*, **19**(1): 191–210.

Ballard C, Gauthier S, Corbett A, et al. 2011. Alzheimer's disease. *The Lancet*, **377**(9770): 1019–1031.

Bayer TA, Cappai R, Masters CL, et al. 1999. It all sticks together—the APP-related family of proteins and Alzheimer's disease. *Molecular Psychiatry*, **4**(6): 524–528.

Blennow K, De Leon MJ, Zetterberg H. 2006. Alzheimer's disease. *The Lancet*, **368**(9533): 387–403.

Brody DL, Holtzman DM. 2006. Morris water maze search strategy analysis in PDAPP mice before and after experimental traumatic brain injury. *Experimental Neurology*, **197**(2): 330–340.

Castelletto V, Ryumin P, Cramer R, et al. 2017. Self-assembly and anti-amyloid cytotoxicity activity of amyloid beta peptide derivatives. *Scientific Reports*, **7**: 43637.

Chen GF, Xu TH, Yan Y, et al. 2017. Amyloid beta: structure, biology and structure-based therapeutic development. *Acta Pharmacologica Sinica*, **38**(9): 1205–1235.

Companys-Alemany J, Turcu AL, Schneider M, et al. 2022. NMDA receptor antagonists reduce amyloid-*β* deposition by modulating calpain-1 signaling and autophagy, rescuing cognitive impairment in 5XFAD mice. *Cellular and Molecular Life Sciences*, **79**(8): 408.

Cooke MB, O'leary TP, Harris P, et al. 2019. Pathfinder: open source software for analyzing spatial navigation search strategies. *F1000Research*, **8**: 1521.

Ding F, Borreguero JM, Buldyrey SV, et al. 2003. Mechanism for the α-helix to β-hairpin transition. *Proteins: Structure, Function, and Bioinformatics*, **53**(2): 220–228.

Feng CL, Yu B, Song C, et al. 2022. Static magnetic fields reduce oxidative stress to improve wound healing and alleviate diabetic complications. *Cells*, **11**(3): 443.

Fish PV, Steadman D, Bayle ED, et al. 2019. New approaches for the treatment of Alzheimer's disease. *Bioorganic & Medicinal Chemistry Letters*, **29**(2): 125–133.

Frachini ECG, Silva JB, Fornaciari B, et al. 2024. Static magnetic field reduces intracellular ROS levels and protects cells against peroxide-induced damage: suggested roles for catalase. *Neurotoxicity Research*, **42**(1): 2.

Fu AKY, Hung KW, Yuen MYF, et al. 2016. IL-33 ameliorates Alzheimer's disease-like pathology and cognitive decline. *Proceedings of the National Academy of Sciences of the United States of America*, **113**(19): E2705–E2713.

Gauthier S, Rosa-Neto P, Morais JA, et al. 2021. World Alzheimer report 2021: journey through the diagnosis of dementia. London: Alzheimer's Disease International.

Graff-Radford J, Yong KXX, Apostolova LG, et al. 2021. New insights into atypical Alzheimer's disease in the era of biomarkers. *The Lancet Neurology*, **20**(3): 222–234.

Hansen DV, Hanson JE, Sheng M. 2018. Microglia in Alzheimer's disease. *Journal of Cell Biology*, **217**(2): 459–472.

Hickman SE, Allison EK, El Khoury J. 2008. Microglial dysfunction and defective β-amyloid clearance pathways in aging Alzheimer's disease mice. *Journal of Neuroscience*, **28**(33): 8354–8360.

Hill RJA, Sedman VL, Allen S, et al. 2007. Alignment of aromatic peptide tubes in strong magnetic fields. *Advanced Materials*, **19**(24): 4474–4479.

Huang ZL, Tan T, Du YH, et al. 2017. Low-frequency repetitive transcranial magnetic stimulation ameliorates cognitive function and synaptic plasticity in APP23/PS45 mouse model of Alzheimer's disease. *Frontiers in Aging Neuroscience*, **9**: 292.

Iwatsubo T, Mann DMA, Odaka A, et al. 1995. Amyloid β protein (Aβ) deposition: Aβ42(43) precedes Aβ40 in down syndrome. *Annals of Neurology*, **37**(3): 294–299.

Ji XM, Tian XF, Feng SA, et al. 2023. Intermittent F-actin perturbations by magnetic fields inhibit breast cancer metastasis. *Research*, **6**: 0080.

Karthivashan G, Ganesan P, Park SY, et al. 2018. Therapeutic strategies and nano-drug delivery applications in management of ageing Alzheimer's disease. *Drug Delivery*, **25**(1): 307–320.

Kaur A, Kaur A, Goyal D, et al. 2020. How does the mono-triazole derivative modulate $A\beta_{42}$ aggregation and disrupt a protofibril structure: insights from molecular dynamics simulations. *ACS Omega*, **5**(25): 15606–15619.

Kleiner DE, Brunt EM, Van Natta M, et al. 2005. Design and validation of a histological scoring system for nonalcoholic fatty liver disease. *Hepatology*, **41**(6): 1313–1321.

Kwon S, Kim BJ, Lim HK, et al. 2015. Magnetotactic molecular architectures from self-assembly of β-peptide foldamers. *Nature Communications*, **6**(1): 8747.

Lehtinen MK, Bonni A. 2006. Modeling oxidative stress in the central nervous system. *Current Molecular Medicine*, **6**(8): 871–881.

Liu FF, Zhao WP, Zhao F, et al. 2020. Dual effect of the acidic polysaccharose ulvan on the inhibition of Amyloid-β protein fibrillation and disintegration of mature fibrils. *ACS Applied Materials & Interfaces*, **12**(37): 41167–41176.

Michaels TCT, Šarić A, Habchi J, et al. 2018. Chemical kinetics for bridging molecular mechanisms and macroscopic measurements of amyloid fibril formation. *Annual Review of Physical Chemistry*, **69**: 273–298.

Pauling L. 1979. Diamagnetic anisotropy of the peptide group. *Proceedings of the National Academy of Sciences of the United States of America*, **76**(5): 2293–2294.

Pugh PL, Richardson JC, Bate ST, et al. 2007. Non-cognitive behaviours in an APP/PS1 transgenic model of Alzheimer's disease. *Behavioural Brain Research*, **178**(1): 18–28.

Pujadas L, Rossi D, Andrés R, et al. 2014. Reelin delays amyloid-beta fibril formation and rescues cognitive deficits in a model of Alzheimer's disease. *Nature Communications*, **5**: 3443.

Saikia J, Pandey G, Sasidharan S, et al. 2019. Electric field disruption of amyloid aggregation: potential noninvasive therapy for Alzheimer's disease. *ACS Chemical Neuroscience*, **10**(5): 2250–2262.

Schieber M, Chandel NS. 2014. ROS function in redox signaling and

oxidative stress. *Current Biology*, **24**(10): R453–R462.
Selkoe DJ. 2001. Alzheimer's disease: genes, proteins, and therapy. *Physiological Reviews*, **81**(2): 741–766.
Singh RK. 2020. Recent trends in the management of Alzheimer's disease: current therapeutic options and drug repurposing approaches. *Current Neuropharmacology*, **18**(9): 868–882.
Tiwari S, Atluri V, Kaushik A, et al. 2019. Alzheimer's disease: pathogenesis, diagnostics, and therapeutics. *International Journal of Nanomedicine*, **14**: 5541–5554.
Todorova N, Bentvelzen A, English NJ, et al. 2016. Electromagnetic-field effects on structure and dynamics of amyloidogenic peptides. *The Journal of Chemical Physics*, **144**(8): 085101.
Yang SH, Lee DK, Shin J, et al. 2017. Nec-1 alleviates cognitive impairment with reduction of Aβ and tau abnormalities in APP/PS1 mice. *EMBO Molecular Medicine*, **9**(1): 61–77.
Younan ND, Viles JH. 2015. A comparison of three fluorophores for the detection of amyloid fibers and prefibrillar oligomeric assemblies. ThT (Thioflavin T); ANS (1-Anilinonaphthalene-8-sulfonic Acid); and bisANS (4, 4'-Dianilino-1, 1'-binaphthyl-5, 5'-disulfonic acid). *Biochemistry*, **54**(28): 4297–4306.
Yu B, Song C, Feng CL, et al. 2023. Effects of gradient high-field static magnetic fields on diabetic mice. *Zoological Research*, **44**(2): 249–258.
Zhang PS, Kishimoto Y, Grammatikakis I, et al. 2019. Senolytic therapy alleviates Aβ-associated oligodendrocyte progenitor cell senescence and cognitive deficits in an Alzheimer's disease model. *Nature Neuroscience*, **22**(5): 719–728.